



Kelvin Waves, Mutual Friction, and Fluctuations in the Gross–Pitaevskii Model

Giorgio Krstulovic¹ · Marc E. Brachet²

Received: 28 April 2023 / Accepted: 27 June 2023

© The Author(s), under exclusive licence to Springer Science+Business Media, LLC, part of Springer Nature 2023

Abstract

In this work, we first briefly review some of the mutual friction effects on vortex lines and rings that were obtained in the context of the truncated Gross–Pitaevskii equation in references Krstulovic and Brachet (Phys Rev E 83(6):066311, 2011; Phys Rev B 83:132506, 2011), with particular attention to the anomalous slowdown of rings produced by thermally excited Kelvin waves. We then study the effect of mutual friction on the relaxation and fluctuations of Kelvin waves on straight vortex lines by comparing the results of full 3D direct simulations of the truncated Gross–Pitaevskii equation with a simple stochastic Local-Induction-Approximation model with mutual friction and thermal noise included. This new model allows us to determine the mutual friction coefficient α and α' for the truncated Gross–Pitaevskii equation.

Keywords Superfluidity · Quantum vortices · Mutual friction · Kelvin waves

1 Introduction

Our knowledge and understanding of the physics of superfluid helium and quantum turbulence has greatly progressed [1]. However, at present, there is no single theory that comprehensively describes all the systems and can predict the observed effects

Giorgio Krstulovic and Marc E. Brachet contributed equally to this work.

✉ Giorgio Krstulovic
krstulovic@oca.eu

Marc E. Brachet
brachet@phys.ens.fr

¹ Laboratoire Lagrange, Observatoire de la Côte d’Azur, CNRS, Université Côte d’Azur, Bd de l’Observatoire, CS 34229, 06304 Nice Cedex 4, France

² Laboratoire de Physique de l’Ecole Normale Supérieure, ENS, Université PSL, CNRS, Sorbonne Université, Université de Paris, 75005 Paris, France

across all length and time scales. Therefore, much of the progress in this field relies on phenomenological models, which may be better suited for certain types of problems than others, and are of several types.

- The phenomenological two-fluid model, proposed independently by L. Tisza and L. Landau, considers the fluid as a mixture of two components: the superfluid and the normal fluid. It successfully describes many flow properties of superfluid helium, including the propagation of second sound. However, it does not account for the presence of quantised vortices, which are an important feature of quantum flows, and were experimentally discovered to have a circulation of h/m by Vinen in 1961 [2].
- An extension of the two-fluid model is the Hall-Vinen-Bekharevich-Khalatnikov model [3–5], which includes the effect of interactions between quantised vortices and the normal fluid through a mutual friction term. However, this model ignores the distinction between individual vortices and only considers length scales larger than the mean separation between vortices, making it an effective, coarse-grained model suitable for describing superfluid turbulence at low Mach numbers.
- The vortex filament model [6, 7] overcomes some of the limitations of the two-fluid and HVBK models by treating the quantised vortices as filaments in three dimensions and evolving them under the Biot-Savart law plus a mutual friction term that mimics the coupling between the normal and superfluid components. In this model, quantum vortex reconnection is implemented by an ad hoc algorithm and the normal fluid is assumed as given and quantum vortices do not modify it.
- The self-consistent vortex filament and Navier–Stokes models [8–11]. This approach allows to account for the mutual interaction of vortices and the normal fluid.
- Finally, at zero or near-zero temperatures, and for weakly interacting bosons, the Gross–Pitaevskii (GP) equation provides a good hydrodynamical description of a quantum flow, that naturally includes quantum vortices as exact solutions which can reconnect.

A problem with the GP model is that including finite temperature effects can be difficult [12–15]. Note that, to the best of our knowledge, only a few attempts [16, 17] have been made to self-consistently couple the Gross–Pitaevskii equation to a Navier–Stokes description of the normal fluid.

In the present study, a minimalistic approach is used by considering classical field models, which involve spectrally truncating the GP Eq. [18]. Long time integration of the truncated system results in microcanonical equilibrium states that can capture a condensation transition, which has been previously demonstrated [19]. The same transition was later reproduced using a grand-canonical method, where it was shown to be a standard second-order λ -transition [20]. This approach also correctly captures dynamical counterflow effects on vortex motion, such as mutual friction and thermalisation dynamics, which have been investigated in previous studies [20, 21].

This manuscript begins by offering a concise review of the mutual friction effects on vortex lines and rings, that were observed in our previous numerical studies. Subsequently, we present new, original results that are obtained by performing full 3D simulations of the truncated Gross–Pitaevskii equation. Focusing on the behaviour of vortex lines, these results are then compared to those derived from a simplified stochastic Local-Induction-Approximation model. This paper is structured as follows: In Sect. 2, we provide a detailed explanation of the GP model and its numerical implementation. Specifically, in Sect. 2.1, we discuss the basic zero-temperature GP theory and its conserved energies. We also introduce and discuss the properties of Kelvin waves propagating along quantum vortices. In Sect. 2.2, we review our spectral truncation methods for incorporating finite-temperature effects, which were developed in reference [20]. We demonstrate the equivalence between the micro-canonical and canonical statistical ensembles in Sect. 2.3. Section 3 reviews our previous findings on mutual friction in lines and rings, as presented in references [22] and [20]. Specifically, standard effects are found for lines in Sect. 3.1, while rings are shown to undergo an anomalous slowdown, produced by thermally excited fluctuating Kelvin waves, in Sect. 3.2. Our new results on fluctuations of Kelvin waves and mutual friction in the spectrally truncated Gross–Pitaevskii model are presented in Sect. 4. We recall the simple zero-temperature LIA model in Sect. 4.1. We present direct simulations of the finite-temperature spectrally truncated GP model in Sect. 4.2. Noise and mutual friction terms are added to the simple zero-temperature LIA model in order to generate KW fluctuation in a Langevin effective model in Sect. 4.3. We relate the observed truncated GP fluctuation and relaxation to the simple Langevin effective model in Sect. 4.4. Finally, our results are discussed and some conclusions are given in Sect. 5.

2 Finite Temperature States in Truncated Gross–Pitaevskii Equation

2.1 The Basic GPE Model

The GP equation [23, 24] is the partial differential equation for the system’s (complex) wave-function ψ that reads

$$i\hbar \frac{\partial \psi}{\partial t} = -\frac{\hbar^2}{2m} \nabla^2 \psi + g|\psi|^2 \psi. \quad (1)$$

It describes the dynamics of a zero-temperature dilute superfluid BEC, m is the mass of the bosons, $g = 4\pi\tilde{a}\hbar^2/m$, (\tilde{a} is the s -wave scattering length). Equation (1) admits three conservation laws corresponding to the total (extensive) number of particles $N_p = \int_V n(\mathbf{x}) d^3x$, the total energy $E = \int_V e(\mathbf{x}) d^3x$ and the momentum $\mathbf{P} = \int_V \mathcal{P}(\mathbf{x}) d^3x$, with respective (intensive) densities:

$$n = |\psi|^2, \quad (2)$$

$$e = \frac{\hbar^2}{2m} |\nabla \psi|^2 + \frac{g}{2} |\psi|^4 \quad (3)$$

$$\mathcal{P} = \frac{i\hbar}{2} (\psi \nabla \bar{\psi} - \bar{\psi} \nabla \psi), \quad (4)$$

where the over-line denotes the complex conjugate.

When no zeros of ψ are present, Eq. (1) can be easily mapped into hydrodynamic equations of motion for a compressible irrotational fluid using the Madelung transformation given by

$$\psi(\mathbf{x}, t) = \sqrt{\frac{\rho(\mathbf{x}, t)}{m}} \exp \left[i \frac{m}{\hbar} \phi(\mathbf{x}, t) \right], \quad (5)$$

where $\rho(\mathbf{x}, t)$ is the fluid density, and $\phi(\mathbf{x}, t)$ is the velocity potential such that the fluid velocity is $\mathbf{v} = \nabla \phi$. The Madelung transformation is singular on the zeros of ψ , which can correspond to topological defects for the phase of the wave-function.

In the absence of vortices, Eq. (1) can be linearised around a constant state $\psi = A_0$. One obtains the Bogoliubov dispersion relation

$$\omega_B(k) = \sqrt{\frac{gk^2 |A_0|^2}{m} + \frac{\hbar^2 k^4}{4m^2}}. \quad (6)$$

The sound velocity is thus given by $c = \sqrt{g|A_0|^2/m}$, with dispersive effects taking place for length scales smaller than the coherence length defined by

$$\xi = \sqrt{\hbar^2 / (2gm|A_0|^2)}; \quad (7)$$

ξ is also proportional to the radius of the vortex cores [25, 26]. When no vortex is present, the GP dynamics is similar to the compressible Euler dynamics, but with the addition of small-scale dispersive effects. These dispersive effects are enough to not allow singularities that are present in the Euler case [27]. In general, the 3D GPE is known to have regular solutions [28].

When quantum vortices are present, the velocity field can be directly obtained as

$$\mathbf{v} = \frac{\mathcal{P}}{n}, \quad (8)$$

The flow matches the behaviour of a classical, ideal, and compressible potential fluid, except at the topological singularities: the so-called quantum vortex lines with quantised Onsager-Feynman velocity circulation given by $\Gamma = \oint_C \mathbf{v}(\ell) d\ell = \frac{\hbar}{m}$, where \mathbf{v} is the superfluid velocity. The vorticity $\omega = \nabla \times \mathbf{v}$ of the flow is thus given by

$$\omega(\mathbf{r}) = \Gamma \int d\zeta \frac{d\mathbf{s}'}{d\zeta} \delta^{(3)}(\mathbf{r} - \mathbf{s}'(\zeta)), \quad (9)$$

where $s(\zeta)$ is the position of the vortex lines and ζ the arc-length. Note that the vorticity is non-zero although $\mathbf{v} = \nabla\phi$, because the phase is not singled value due to the topological defects produced by the zeros of ψ .

The simplest hydrodynamic excitations of a quantum vortex are dispersive heliocidal perturbations of the filament, known as Kelvin waves [24, 29]. They were first studied by Lord Kelvin in 1880 [30] using the incompressible Euler equations. In the case of a hollow vortex core, such waves propagate with the dispersion relation

$$\omega_k^{KW} = \frac{\Gamma}{2\pi a_0^2} \left(1 \pm \sqrt{1 + ka_0 \frac{K_0(ka)}{K_1(ka_0)}} \right)_{a_0 k \ll 1} \approx -\frac{\Gamma}{4\pi} k^2 \left(\ln \frac{2}{a_0 k} - \gamma_E \right), \quad (10)$$

where k is the wavenumber, a_0 is a constant of the order of the vortex core radius, $\gamma_E \approx 0.5772$ is the Euler-Mascheroni constant, and K_0 and K_1 are the modified Bessel functions. Note that their frequencies have the opposite sign with respect to the circulation Γ .

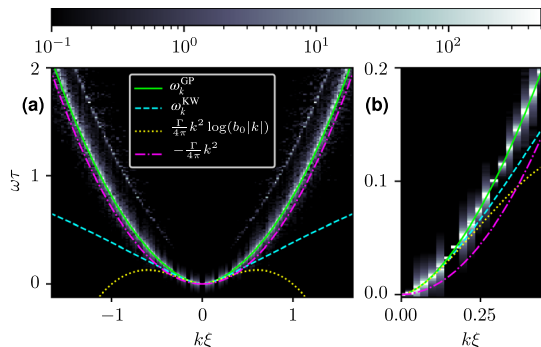
In the case of the GP model, the dispersion relation was first derived in the limit $a_0 k \ll 1$ by Pitaevskii [24] and then improved by P.H. Roberts [31]. Robert’s work allows to fix the constant of the core value to $a_0 = 1.1265\xi$. However, P.H. Roberts also showed that in the opposite limit of large wave vectors, the vortex wave dispersion relation scales as k^2 , which is not in agreement with the scaling $\omega_k^{KW} \sim k^{1/2}$ for large k . In order to conciliate both scalings, reference [32] proposed a fit that matches both scaling laws. Such a fit was useful to perform analytical calculations and to analyse data. The whole dispersion relation of the GP is well represented by

$$\omega_k^{GP} = \omega_k^{KW} \times \left[1 + \epsilon_{\frac{1}{2}} (a_0 k)^{1/2} + \epsilon_1 (a_0 k) + \frac{1}{2} (a_0 k)^{3/2} \right], \quad (11)$$

where $\epsilon_{\frac{1}{2}} = -0.20$ and $\epsilon_1 = 0.64$ are two fitting parameters. The last term of the expansion is fixed to match the $a_0 k \gg 1$ GP asymptotic limit. Finally, note that in the simplest KW description given by the Local-Induction-Approximation (LIA) [33] (see also Sect. 4.1), the \log -term is ignored and treated as a constant.

Figure 1, reproduced from reference [32], shows the measured KW dispersion relation in GP simulations and different theoretical predictions.

Fig. 1 Figure reproduced from reference [32]. **(a)** Kelvin wave dispersion relation obtained from GP simulations. All theoretical predictions are also displayed for comparison. **(b)** A zoom for $k\xi \ll 1$ where the logarithmic correction can be appreciated. Details on the numerical simulations can be found in [32]



2.2 Truncation and Conserved Quantities

The truncated Gross–Pitaevskii (TGP) equation is obtained from the GP model by truncating the Fourier transform of the wave-function ψ : $\hat{\psi}_{\mathbf{k}} \equiv 0$ for $|\mathbf{k}| > k_{\max}$ [18, 19]. Introducing the Galerkin projector \mathcal{P}_G that reads in Fourier space $\mathcal{P}_G[\hat{\psi}_{\mathbf{k}}] = \theta(k_{\max} - |\mathbf{k}|)\hat{\psi}_{\mathbf{k}}$ with $\theta(\cdot)$ the Heaviside function, the TGP equation explicitly reads

$$i\hbar \frac{\partial \psi}{\partial t} = \mathcal{P}_G \left[-\frac{\hbar^2}{2m} \nabla^2 \psi + g \mathcal{P}_G[|\psi|^2] \psi \right]. \quad (12)$$

The truncation of the GP equation preserves its Hamiltonian structure. The corresponding Hamiltonian is $H_{\text{TGP}} = \int \mathcal{P}_G \left[\frac{\hbar^2}{2m} |\nabla \psi|^2 + \frac{g}{2} (\mathcal{P}_G[|\psi|^2])^2 \right] d^3x$. The outermost projector can be omitted if we assume that initially $\mathcal{P}_G \psi = \psi$. Equation (12) can be thus rewritten in the canonical way as $i\hbar \frac{\partial \psi}{\partial t} = \frac{\delta H_{\text{TGP}}}{\delta \psi^*}$. It follows that energy and mass are conserved by (12) as the time and $U(1)$ invariances are preserved in H_{TGP} . Conservation of momentum is also preserved when standard Fourier pseudo-spectral methods are used, provided that they are dealiased using the 2/3-rule ($k_{\max} = 2/3 \times M/2$ [34] at resolution M). In this scheme, to achieve conservation mass and momentum are, respectively, evaluated as in (2), (4) and the energy (3) must be evaluated as in $e = \frac{\hbar^2}{2m} |\nabla \psi|^2 + \frac{g}{2} [\mathcal{P}_G[|\psi|^2]]^2$. Note that global momentum conservation is mandatory to correctly describe vortex-normal fluid interactions. When the nonlinear term in Eq. (12) is written, as in [19], $\mathcal{P}_G[|\psi|^2 \psi]$ momentum conservation requires that the dealiasing must be performed at $k_{\max} = M/4$ (see reference [20] and [35] for details).

Note that when the wavefunction ψ is an analytical function (or more regular), it decreases very rapidly in Fourier space with the magnitude of the wave number (typically exponentially or faster). In that case, and provided that k_{\max} is much larger than the largest active wavenumber of ψ , the GP and TGP equations coincide. This criterion is called spectral accuracy and should be fulfilled while solving a partial differential equation. On the contrary, the TGP model allows for solutions which do not decay at large wave numbers, which typically correspond to the thermal states discussed in the next section. As fields do not decrease for large wave numbers, they are not differentiable at any point. Formally speaking, the TGP is not a partial differential equation but a high-dimensional ordinary differential equation.

2.3 Equivalence Micro- and Grand-Canonical Thermalisation

Microcanonical equilibrium states are produced by integration of TGP equation for very long times [19, 36, 37]. On the other hand, grand-canonical states are defined by the probability distribution

$$\mathbb{P}_{\text{st}}[\psi] = \mathcal{Z}^{-1} \exp[-\beta E - \mu N] \tag{13}$$

directly expressed in terms of the temperature β^{-1} and the chemical potential μ (instead of the energy E and the number of particles N in a microcanonical framework). These states can be efficiently obtained by constructing a stochastic process that converges to a realisation with the probability $\mathbb{P}_{\text{st}}[\psi]$ [20]. This process is defined by a Langevin equation consisting in a stochastic Ginzburg-Landau equation (SGLE):

$$\hbar \frac{\partial \psi}{\partial t} = \mathcal{P}_G \left[\frac{\hbar^2}{2m} \nabla^2 \psi + \mu \psi - g \mathcal{P}_G[|\psi|^2] \psi \right] + \sqrt{\frac{2\hbar}{V\beta}} \mathcal{P}_G[\zeta(\mathbf{x}, t)], \tag{14}$$

where the white noise $\zeta(\mathbf{x}, t)$ satisfies $\langle \zeta(\mathbf{x}, t) \zeta^*(\mathbf{x}', t') \rangle = \delta(t - t') \delta(\mathbf{x} - \mathbf{x}')$, β is the inverse temperature and μ the chemical potential. Using this algorithm in [20] the microcanonical and grand-canonical ensembles were shown to be equivalent and the condensation transition reported in [19, 36] identified with the standard second order λ -transition.

When numerically simulating Eq. (14), μ is adjusted to fix the density. The inverse temperature is normalised as $\beta = \mathcal{N}/VT$, where \mathcal{N} is the total number of Fourier modes and V the system volume. With this choice of parametrization the λ -transition temperature T_λ is independent of \mathcal{N} . Data from SGLE and low-temperature calculations obtained in reference [20] are shown in Fig. 2.

The temperature dependence of the different energies is also displayed in Fig. 2. Note that the first term in Eq. (3) that defines the energy can be decomposed (as done in [25, 26]) into incompressible E_{kin}^i , and compressible E_{kin}^c kinetic energies and into quantum energies E_q . The last term in Eq. (3) corresponds to the internal energy E_{int} . Observe that E_{kin}^i vanishes at temperatures $T/T_\lambda \lesssim 1/2$. At low temperature equipartition of energy between E_{kin} and $E_q + E_{\text{int}}$ is apparent.

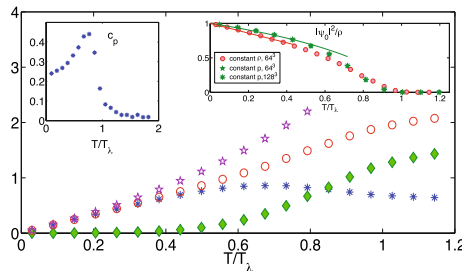


Fig. 2 This figure, reproduced from [21], shows the temperature dependence of various energies: E_{kin}^c (stars), E_{kin}^i (diamonds), E_{kin} (circles), and $E_q + E_{\text{int}}$ (pentagrams) at constant density. The insets show the temperature dependence of the condensate fraction $|\psi_0|^2/\rho$ (right) and the specific heat $c_p = \frac{\partial H}{\partial T} \Big|_p$ at a resolution of 128^3 (left). Note that E_{kin}^i denotes the presence of vortices (see text). Details on the numerical simulations can be found in [21]

Such a behaviour suggests that thermally excited quantum vortices are important for temperatures larger than $T_\lambda/2$.

Adding $-\mathbf{v}_n \cdot \mathbf{P}$ as a Lagrange multiplier to the grand-canonical distribution (13) and correspondingly a term $i\hbar \mathbf{v}_n \cdot \nabla\psi$ in (14) induces an asymmetry in the repartition of thermal waves and generates non-zero momentum states. These states do not generally correspond to a condensate moving at velocity $\mathbf{v}_s = \mathbf{v}_n$ because \mathbf{v}_s is the gradient of a phase and takes discrete values for finite size systems. Equilibrium states with nonzero values of the counterflow $\mathbf{w} = \mathbf{v}_n - \mathbf{v}_s$ are generated in this way.

All the SGLE equilibrium used in this work has a condensate at rest ($\mathbf{v}_s = \mathbf{0}$) and therefore $\mathbf{v}_n = \mathbf{w}$.

3 Vortex Lines at Finite Temperature

In this section, we review the results on mutual friction obtained in references [20] and reference [22].

3.1 Mutual Friction in the Truncated Gross–Pitaevskii Model

We start by recalling the standard Hall-Vinen phenomenological model for the vortex line velocity \mathbf{v}_L [3, 4, 29] that reads:

$$\mathbf{v}_L = \mathbf{v}_{sl} + \alpha \mathbf{s}' \times (\mathbf{v}_n - \mathbf{v}_{sl}) - \alpha' \mathbf{s}' \times [\mathbf{s}' \times (\mathbf{v}_n - \mathbf{v}_{sl})], \quad (15)$$

where \mathbf{s}' is the tangent of the vortex line, $\mathbf{v}_{sl} = \mathbf{v}_s + \mathbf{u}_i$ is the local superfluid velocity with \mathbf{u}_i the self-induced vortex velocity and \mathbf{v}_n the normal velocity. The mutual friction coefficients in Eq. (15) are typically written as $\alpha = B\rho_n/2\rho$, $\alpha' = B'\rho_n/2\rho$ where B and B' are order-one and weakly temperature-dependent.

In reference [22] we used the TGP model to study the effect of mutual friction on an array of alternate-sign straight vortices ψ_{lattice} , which is an exact stationary solution of the GP equation (for details on this initial data, see [20] and also [38]). We set an initial condition where the vortices were separated by a distance $L/2$ (L being the system size) and thus they can be considered isolated for a large enough box. An equilibrium state ψ_{eq} was also generated with the SGLE (14) with counterflow v_n perpendicular to the vortices. The initial condition $\psi = \psi_{\text{lattice}} \times \psi_{\text{eq}}$ was then evolved with the TGP equation.

Figure 3a displays 3D visualisations of the density at $t = 0$ and $t = 100$, where the displacement of the lattice is apparent (figure reproduced from [22]).

The temporal evolution of the (parallel and perpendicular to \mathbf{v}_n) position of a vortex (R_{\parallel}, R_{\perp}) is presented in Fig. 3c for $T = 0.2T_\lambda$, $T = 0.4T_\lambda$ and $v_n = 0.4$. The counterflow-induced vortex velocity clearly depends on the temperature. R_{\parallel} has a linear behaviour, that allows to directly measure the parallel velocity v_{\parallel} . The temperature dependence of v_{\parallel}/v_n is presented later on Fig. 5 for different values of v_n and ξ . This behaviour is consistent with the standard phenomenological model

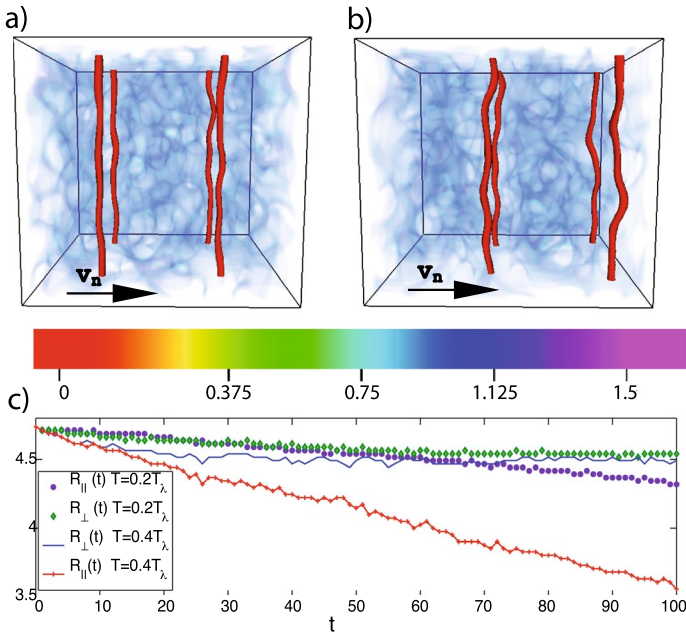


Fig. 3 The figure, reproduced from reference [22], displays three panels: **a** and **b** show the density distribution at $t = 0$ and $t = 100$, respectively, for the lattice configuration (in red) with $T = 0.4, T_{\lambda}$ and $v_n = 0.4$, where the blue clouds correspond to density fluctuations. Panel **c** shows the averaged positions (R_{\parallel}, R_{\perp}) of a single vortex for different temperatures ($T = 0.2, T_{\lambda}$ and $T = 0.4, T_{\lambda}$) and $v_n = 0.4$. The resolution used in this figure was 64^3 . Details on the numerical simulations and method used can be found in [22]

for the vortex line velocity \mathbf{v}_L (15), as Eq. (15) applied to a straight vortex with v_n perpendicular to the vortex and $v_s = 0$ yields $\alpha' = v_{\parallel}/v_n$.

3.2 Slowdown Effect on Vortex Rings Induced by Thermal Fluctuations

Let us now rapidly review the interaction of vortex rings and counterflow. The Biot-Savart self-induced velocity of a perfectly circular vortex ring of radius R is given by

$$u_i = \frac{\hbar}{2m} \frac{C(R/\xi)}{R}, \quad C(z) = \ln(8z) - a \tag{16}$$

where a is a core model-dependent constant [29].

Equation (15) with v_n perpendicular to the ring, and $v_s = 0$ yields the radial velocity $\dot{R} = -\alpha(u_i - v_n)$. Using the TGP model, Berloff and Youd [37] studied the finite temperature evolution of a ring without counterflow ($v_n = 0$) and observed a contraction of vortex rings compatible with (15). To study the influence of counterflow, in reference [22] we prepared an initial condition $\psi = \psi_{\text{ring}} \times \psi_{\text{eq}}$ in the

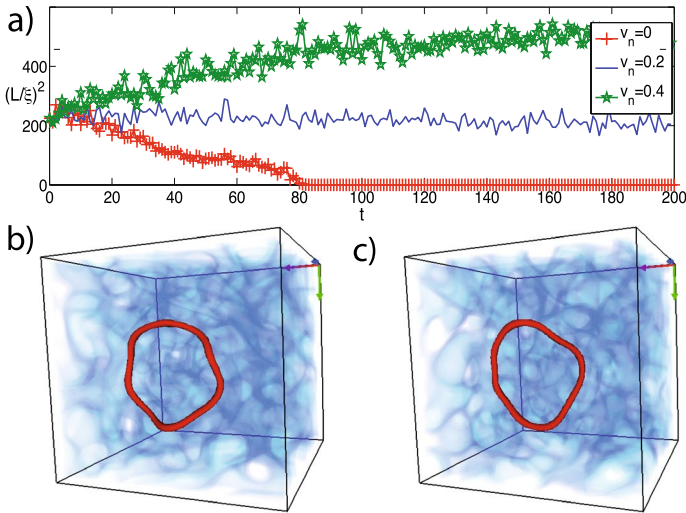


Fig. 4 Figure reproduced from reference [22]. **a** The (squared) length of a vortex ring at different values of counterflow v_n as a function of time (temperature $T = 0.4 T_\lambda$ and initial radius $R = 15\xi$). **b–c** 3D visualisations of a vortex ring ($R = 20\xi$) and density fluctuations at $t = 18, 19$ with $T = 0.4 T_\lambda$ and resolution 64^3 . The same colour bar as in Fig. 3 is used. Thermally excited Kelvin waves can be seen. Details on the numerical simulations can be found in [22]

same way as above for the vortex lattice. The temporal evolution of the (squared) vortex length of a ring of initial radius $R = 15\xi$ at temperature $T = 0.4 T_\lambda$ and $v_n = 0, 0.2$ and 0.4 is reproduced in Fig. 4a. The Berloff-Youd contraction [37] is apparent in absence of counterflow (bottom curve). The temperature dependence of the contraction, related to the α coefficient in Eq. (15), also quantitatively agrees with their published results (data not shown).

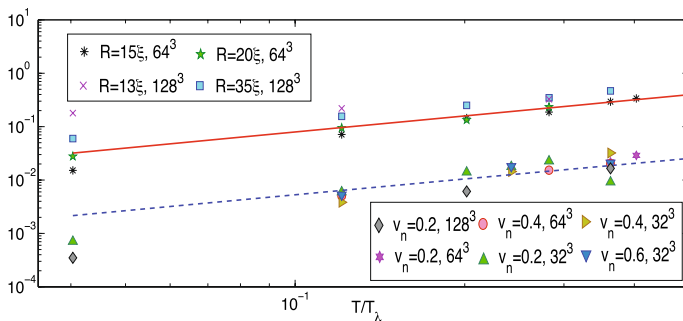


Fig. 5 This figure is reproduced from reference [22]. It shows the temperature dependence of the counterflow-induced lattice velocity $v_{||}/v_n$ (bottom) and ring slowdown $\Delta v_L/u_i$ (top) obtained with $v_n = 0$. The dashed line represents the prediction of Eq. (15) with $\alpha' = 0.83\rho_n/2\rho$, while the solid line shows the prediction of anomalous slowdown by Eq. (18) with $R = 20\xi$ at various resolutions. Details on the numerical simulations can be found in [22]

When the counterflow was large enough, a dilatation of vortex rings was instead observed (top curve in Fig. 4a). Such a dilatation (a hallmark of counterflow effects) is expected [29] to correspond to a change of sign of $\mathbf{v}_n - \mathbf{v}_{sl}$ in Eq. (15). The predictions of Eq. (15) unexpectedly turned out to be quantitatively wrong. Indeed, using Eq. (16) in the conditions of Fig. 4a one finds that $\mathbf{v}_{sl} = \mathbf{u}_i = 0.39$ which is significantly larger than normal velocity $v_n = 0.2$ around which dilatation starts to take place (see the middle curve in Fig. 4a). Equation (15) prediction for the longitudinal velocity $v_L = (1 - \alpha')u_i + \alpha'v_n$ was also unexpectedly found wrong. Using the value of α' determined above on the vortex array, one finds $v_L \sim 0.98u_i$ and from Eq. (16) one finds for v_L the value 0.38 that is larger than the measured value $v_L = 0.23$.

This anomaly of the ring velocity v_L is also present in the absence of counterflow ($v_n = 0$) where Eq. (15) predicts that α' should be given by $\Delta v_L/u_i \equiv (u_i - v_L)/u_i$. The temperature dependence of $\Delta v_L/u_i$, reproduced from [22], is displayed in Fig. 5 (top curve). Observe that $\Delta v_L/u_i$ is one order of magnitude above the transverse mutual friction coefficient α' measured on the lattice.

This unexpected behaviour was related to the presence of thermally excited Kelvin waves in reference [22]. It was known that KWs present in vortex rings slow-down the ring propagation velocity by a purely hydrodynamical effect [39, 40]. As KWs are naturally excited at finite temperatures, they thus could be used to explain this unexpected observed effect. We now reproduce the calculations of [22] of the thermally induced anomaly to the velocity v_a induced on a vortex ring by a single a Kelvin wave of (small) amplitude A and (large) wavenumber $N_K/2\pi R$ obtained in the LIA [39] and Biot-Savart [40] frameworks. The translation velocity v_a obtained in the framework of LIA reads (see Eq. (26) of [39])

$$v_a = u_i(1 - A^2 N_K^2/R^2 + 3A^2/4R^2) \tag{17}$$

where u_i is the (undisturbed) ring velocity (16).

The TGP model naturally includes thermal fluctuations that excite Kelvin waves, as apparent in Fig. 4b, c. We assume that the slowing down effect of each individual Kelvin wave is additive and that the waves populate all the possible modes. Kelvin waves being bending oscillations of the quantised vortex lines their wavenumber must satisfy $k \leq k_\xi = 2\pi/\xi$. The total number of thermally excited Kelvin waves is thus $\mathcal{N}_{\text{Kelvin}} \approx R k_\xi$.

The amplitude term $A^2 N_K^2/R^2$ in (17) can be obtained by simple equipartition arguments. The energy of a (perfect) ring is $E = \frac{2\pi^2 \rho_s \hbar^2}{m^2} R[C(R/\xi) - 1]$, with ρ_s the superfluid density [29]. A Kelvin wave produces a variation of the ring length $\Delta L = \pi A^2 N_K^2/R$. Its energy can thus be estimated as $\Delta E = \frac{dE}{dR} \frac{\Delta L}{2\pi}$. Assuming $\Delta E = \beta^{-1}$ yields, at low temperature where $\rho_s \approx \rho$, $A^2 N_K^2/R^2 = m^2 \beta^{-1} / \pi^2 \rho \hbar^2 R C(R/\xi)$. Note that this formula predicts a UV-convergent r.m.s amplitude that is in good agreement with TGP data, with values small enough to avoid self-reconnections of the ring. Replacing A^2/R^2 in Eq. (17), the dominant effect is obtained by summing up to $\mathcal{N}_{\text{Kelvin}}$ and it finally reads:

$$\frac{\Delta v_L}{u_i} \equiv \frac{u_i - v_a}{u_i} \approx \frac{\beta^{-1} m^2}{\pi^2 \rho \hbar^2 C(R/\xi)} k_\xi. \quad (18)$$

The thermally induced anomalous slowdown (18) is in good agreement with the TGP data displayed in Fig. 5.

4 Fluctuation and Relaxation of Kelvin Waves in Thermal Equilibrium

When the standard LIA description of Kelvin waves is used together with the Hall-Vinen [3, 4] phenomenological description of mutual friction, the normal fluid velocity appears naturally as an external variable that is given independently of the vortex positions. We have seen that the TGP model naturally includes thermal fluctuations that excite Kelvin waves. Such random thermal perturbations are physically expected to occur in nature and not only in the TGP model.

In this section, we review the description of KWs in the LIA model, their expected energy equipartition at finite temperatures, and build a simple Langevin model of the effect of thermal perturbations by including random fluctuations in the normal fluid velocity. We will be specially interested in the fluctuations and relaxation of thermally excited Kelvin waves.

4.1 Description of Kelvin Waves at $T = 0$ Using the Local-Induction-Approximation

The simplest description of Kelvin wave dynamics is given by the local induction approximation (LIA) [33], in which only local contributions of the Biot-Savart integrals in the Schwarz vortex filament model [6, 7] are considered. In the zero-temperature limit, the LIA equations are simply given by

$$\dot{\mathbf{s}} = -\frac{\Gamma\Lambda}{2\pi} \mathbf{s}' \times \mathbf{s}'' \quad (19)$$

where \mathbf{s} denotes, as in (15), the parametrisation of a vortex line. The vortex circulation is given by Γ and the constant $\Lambda = \log(\ell/a_0)$, with ℓ the inter-vortex distance and a_0 the vortex core size.

In the particular case of small amplitude Kelvin waves, the vortex parametrisation takes a simpler form using Cartesian coordinates. For a vortex line aligned along the z -direction, the vortex can be parametrised as $\mathbf{s}(z) = (X(z), Y(z), z)$. Furthermore, by introducing the complex amplitude $s(z) = X(z) + iY(z)$, and taking the limit of small amplitudes, the LIA equations become

$$i\dot{s} = -\frac{\Gamma\Lambda}{4\pi} \frac{\partial^2 s}{\partial z^2}. \quad (20)$$

Note that the previous equation is equivalent to the (linear) Schrödinger equation. In particular, note that in the LIA approximation, KWs have a dispersion relation

$$\omega_k^{\text{LIA}} = -\frac{\Gamma\Lambda}{4\pi}k^2, \tag{21}$$

where k is the wave vector. Although the LIA equations fail to give the correct large-scale asymptotic dispersion relation (10), it is a useful theoretical tool to perform analytical calculations and comparison with the GP model [32, 41].

The LIA equations have a Hamiltonian structure in which energy is proportional to the total vortex length. In the case of small KW amplitudes, the energy of the filament is given by

$$H_{\text{LIA}} = \frac{\Gamma^2\Lambda}{4\pi} \int \left| \frac{\partial s}{\partial z} \right|^2 dz = -\Gamma \sum_k \omega_k^{\text{LIA}} |\hat{s}_k|^2, \tag{22}$$

where \hat{s}_k is the Fourier transform of $s(z)$, and for simplicity we have considered a periodic system in the z -direction.

At finite temperatures, and in the absence of external driving, one naturally expects that KWs will be in equilibrium with the thermal bath. More specifically, in the classical approximation, vortex line excitations should obey the Gibbs distribution $\{s(z)\} \sim \exp\{-H_{\text{LIA}}/T\}$, where T is the temperature of the thermal bath. As H_{LIA} is quadratic in s , every Fourier mode will be Gaussian and will be in equipartition. It follows that the thermal KW spectrum is given by

$$n_k = |\hat{s}_k|^2 + |\hat{s}_{-k}|^2 \propto \frac{T}{-\Gamma\omega_k^{\text{LIA}}} \sim \frac{T}{k^2}. \tag{23}$$

The previous considerations are also valid using a more realistic description of linear KWs. For a different model, it is enough to replace ω_k^{LIA} by a more accurate expression of the KW dispersion relation, for instance, the one given by Eq. (11).

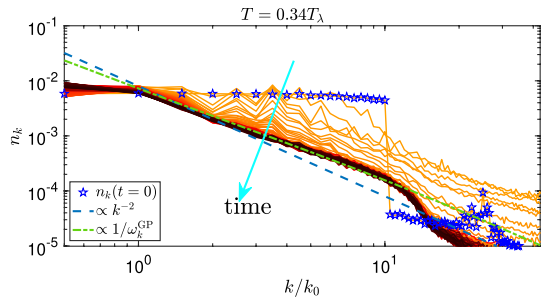
4.2 Finite-Temperature Kelvin Wave Gross–Pitaevskii Simulations

In order to check prediction (23), we study the finite-temperature evolution of an initial non-equilibrium distribution of KWs using the TGP Eq. (12). For a given temperature T , which value will be expressed in terms of the condensation transition temperature T_λ , we first prepare a thermal state ψ^{thermal} . Then, we also prepare a wave function ψ^{KW} containing four (to ensure periodicity) almost straight vortices satisfying

$$s^{\text{ini}}(z) = \sum_{k=-k_m}^{k_m} A e^{ikz+i\phi_k}, \tag{24}$$

where ϕ_k are random phases and A is the KW amplitude. The initial condition is prepared in the same manner as in [42]. Finally, the initial condition $\psi = \psi^{\text{thermal}} \times \psi^{\text{KW}}$ is evolved with the TGP Eq. (12). During the evolution, we track the four vortex lines of the periodic box. In general, tracking KW requires high precision in order to

Fig. 6 Temporal evolution of the Kelvin wave spectrum n_k . The initial condition is highlighted with pentagrams, and the cyan and green dashed line shows the LIA k^{-2} scaling and $1/\omega_k^{\text{GP}}$ prediction (11). k_0 is the smallest wavenumber of the simulation



capture small fluctuations. In the case of GP (not truncated), one can use the regularity of the field and a Newton–Raphson scheme to find the nodal lines of the wave function [42, 43]. This approach is particularly accurate in pseudo-spectral codes thanks to the spectral accuracy of such solvers. As for finite temperature states, the fields are not differentiable. This method and others based on interpolation are not thus applicable. Instead, in this work, we use a simpler scheme where the vortex is determined by finding the minimum the density, after filtering the fields to reduce small-scale fluctuations. As we will say later, this simple method allows for determining statistical quantities with good precision.

In the numerics, we use the pseudo-spectral code FROST [35] with a periodic box of size $L \times L \times 2L$ using $128 \times 128 \times 256$ collocation points and a Runge-Kutta-4 time-marching scheme. Thermal states are prepared at constant density $\rho = 1$. At zero-temperature, the healing length is set to $\xi = 1.5L/128$. Furthermore, as the vortex filaments are highly fluctuating quantities, for each temperature studied in this work, we perform 27 different realisations to improve statistics. As the four vortices can be considered to be statistically independent, this results in a statistical ensemble of more than 100 vortex lines for each temperature. Finally, we prepare an out-of-equilibrium vortex configuration ψ^{KW} , with an almost straight vortex as in Eq. (24) with $k_m = 20k_0$, with $k_0 = \pi/L$. We filter the fields at wave number $k_f = 15k_0$ to track the vortex lines. The amplitude of the KWs is set to $5\xi/\sqrt{2}$.

Figure 6 displays the temporal evolution of the KW spectrum at a temperature $T = 0.34T_\lambda$. Initially, the spectrum is flat and drops at $k = 10k_0$ as set by the initial condition. During the time evolution we observe that the vortex spectrum relaxes towards the equilibrium spectrum (23), displayed by the green dashed line. Note that the LIA prediction provides a reasonable prediction for scaling for small k/k_0 -scaling, but as k/k_0 increases, it deviates from $1/\omega_k^{\text{GP}}$ which reproduces well the data.

We have shown how a simple physical argument can predict the scaling of KW spectrum in equilibrium. However, in order to predict temporal dynamics, one needs to do further modelling. In the next section, we introduce a Langevin model that predicts the temporal behaviour of KWs close to equilibrium.

4.3 Stochastic LIA Equations for Finite Temperature Quantum Vortices

In vortex filament models, finite temperature effects are typically taken into account using the Hall-Vinen Eq. (15). In this framework, the LIA finite-temperature description is obtained by using the self-induced velocity $\mathbf{v}_{sl} = -\frac{\Gamma\Lambda}{2\pi}\mathbf{s}' \times \mathbf{s}''$. It reads

$$\dot{\mathbf{s}} = -\frac{\Gamma\Lambda}{2\pi}\mathbf{s}' \times \mathbf{s}'' + \alpha\mathbf{s}' \times \left(\mathbf{v}_n + \frac{\Gamma\Lambda}{2\pi}\mathbf{s}' \times \mathbf{s}''\right) - \alpha'\mathbf{s}' \times \left[\mathbf{s}' \times \left(\mathbf{v}_n + \frac{\Gamma\Lambda}{2\pi}\mathbf{s}' \times \mathbf{s}''\right)\right], \tag{25}$$

where we recall that α and α' are the mutual friction coefficients and $\mathbf{v}_n = (v_n^1, v_n^2, v_n^3)$ is the prescribed normal fluid. Note that in this model, thermal fluctuations are absent.

We consider now the case of vortex line close to equilibrium at small temperatures, for which Kelvin wave amplitudes and the normal fluid are both small. Similarly to the $T = 0$ case, the linear equations written in complex variables read

$$\frac{\partial s}{\partial t} = -(\alpha + i(\alpha' - 1))\frac{\Gamma\Lambda}{4\pi}\frac{\partial^2 s}{\partial z^2} + (i\alpha + \alpha')U \tag{26}$$

where $U = v_n^1 + iv_n^2$.

We now assume that thermal fluctuations are introduced in the system through the normal fluid. At low-temperatures, and within a classical approximation, the one time-statistics of the thermal bath is Gaussian and each Fourier mode of U can be assumed to be independent. Furthermore, in reference [44], it was shown that the correlation time of thermal states is of order ξ/c , which is much smaller than typical large-scale KW periods. Under this assumption, it is natural then to assume that U is a white noise in time. Rewriting Eq. (26) in Fourier space, and incorporating the previous considerations, leads to the following stochastic local induction approximation (SLIA) equation

$$\frac{\partial \hat{s}_k}{\partial t} = -\gamma k^2 \hat{s}_k + \sigma \zeta(t) \tag{27}$$

$$\langle \zeta(t) \rangle = 0 \tag{28}$$

$$\langle \zeta^*(t)\zeta(t') \rangle = \delta(t - t'), \tag{29}$$

where $\gamma = (\alpha + i(\alpha' - 1))\frac{\Gamma\Lambda}{4\pi}$ and $\sigma^2 = (\alpha^2 + \alpha'^2)\langle |U|^2 \rangle$. Note that γ is a complex number and encompasses damping by mutual friction and oscillations due to KW dynamics. The amplitude of the noise is related to the normal fluid mean kinetic energy, which is proportional to temperature.

The complex Langevin Eq. (27) admits a simple solution in terms of the standard Wiener process W_s . It reads

$$\hat{s}_k(t) = \hat{s}_k(0)e^{-\gamma k^2 t} + \sigma \int_0^t e^{-\gamma k^2(t-s)} dW_s. \tag{30}$$

The above formula allows to directly compute the correlation function of KWs by simple algebra and using basic properties of the Wiener process. The correlation function is given by

$$\begin{aligned} \langle \hat{\delta}_k(t)\hat{\delta}_k^*(t') \rangle &= \langle \hat{\delta}_k(0)\hat{\delta}_k^*(0) \rangle e^{-\gamma k^2 t - \gamma^* k^2 t'} + \sigma^2 \int_0^t \int_0^{t'} e^{-\gamma k^2(t-s) - \gamma^* k^2(t'-s')} \langle dW_s dW_{s'} \rangle \\ &= \langle \hat{\delta}_k(0)\hat{\delta}_k^*(0) \rangle e^{-\gamma k^2 t - \gamma^* k^2 t'} + \sigma^2 \int_0^t e^{-\gamma k^2(t-s') - \gamma^* k^2(t'-s')} ds' \\ &= \langle \hat{\delta}_k(0)\hat{\delta}_k^*(0) \rangle e^{-\gamma k^2 t - \gamma^* k^2 t'} + \frac{\sigma^2 (e^{-2\text{Re}[\gamma]k^2 t - k^2(t\gamma + t'\gamma^*)} - e^{-k^2(t\gamma + t'\gamma^*)})}{2k^2\text{Re}[\gamma]}. \end{aligned} \tag{31}$$

Note that the equipartition spectrum (23) follows from the previous expression by taking $t = t' \rightarrow \infty$

$$\langle |\hat{\delta}_k|^2 \rangle = \frac{\sigma^2 4\pi}{2\alpha \Gamma \Lambda k^2}. \tag{32}$$

The previous expression relates fluctuations (σ) and dissipation (α) of KWs in equilibrium.

More interesting, expression (31) gives an explicit formula for the correlation function

$$C_k(\tau) = \frac{\text{Re}[\langle \hat{\delta}_k(0)\hat{\delta}_k^*(\tau) \rangle]}{\langle |\hat{\delta}_k(0)|^2 \rangle}. \tag{33}$$

Assuming that at $t = 0$ all the KWs are in thermal equilibrium, formula (31) leads to

$$C_k(\tau) = e^{-\alpha \frac{\Gamma \Lambda}{4\pi} k^2 \tau} \cos \left[(\alpha' - 1) \frac{\Gamma \Lambda}{4\pi} k^2 \tau \right]. \tag{34}$$

We expect then a decay rate given by the mutual friction coefficient α and a renormalisation of the KW frequency due to α' .

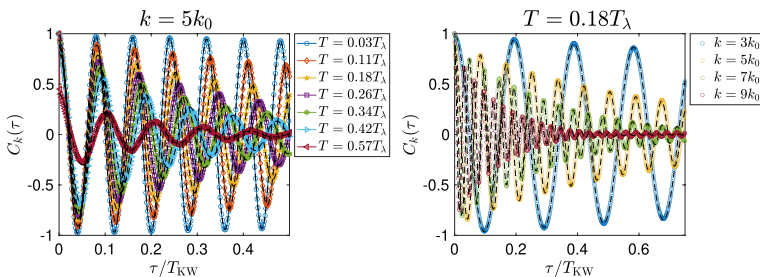


Fig. 7 Equilibrium Kelvin wave correlation function (33) obtained using the TGP equation. **left:** Correlation function at different temperatures for a fixed wave vector. **right:** Correlation function at different wave vectors for a fixed temperature. The dashed lines show the fit obtained using formula (35)

Note that a more realistic description could be obtained by replacing the LIA dispersion relation ω_k^{LIA} by a more accurate KW dispersion in the same spirit of predictions made in [32]. With such a change, Eq. (25) becomes a non-local partial differential equation (with Laplacian replaced by a non-local operator), but with a simple representation in Fourier space and all the previous calculations trivially follow.

4.4 Finite-Temperature Equilibrium Kelvin Wave Correlation Function Using the Truncated Gross–Pitaevskii Model

We now study the correlation function (33) using the TGP equation. We use the same numerical setting of Sect. 4.2 and we compute the correlation function once the KWs have reached thermal equilibrium. The measured correlation functions for different temperatures and wave vectors are displayed in Fig. 7.

It is apparent from the figure that there is a clear temperature-dependent decay rate and a slowdown of the oscillation frequency. The quality of the data allows us to determine damping and frequency coefficients by fitting the temporal series with the fit

$$C_k^{\text{fit}}(\tau) = Ae^{-\lambda_k t} \cos \Omega_k t. \tag{35}$$

The resulting fits are also displayed in Fig. 7 in black dashed lines.

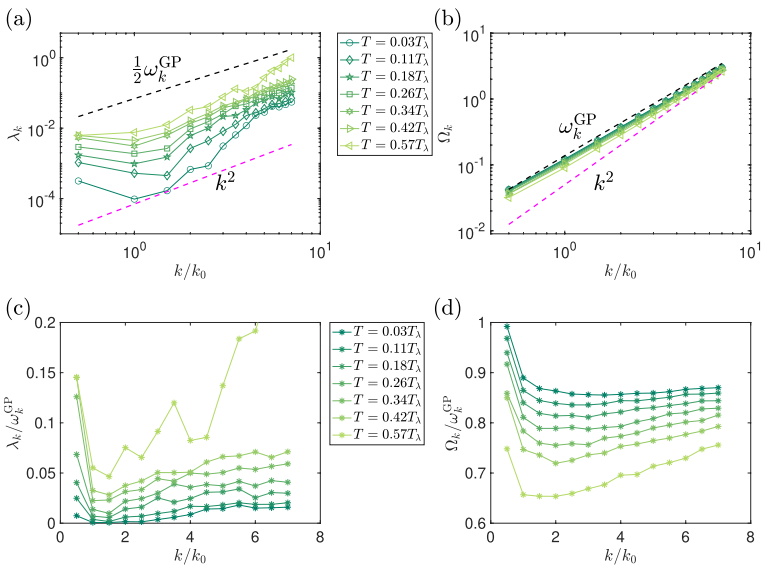


Fig. 8 Equilibrium Kelvin correlation function (33) obtained using the TGP equation. **left:** Correlation function at different temperatures for a fixed wave vector. **right:** Correlation function at different wave vectors for a fixed temperature. The dashed lines show the fit obtained using formula (35) (factor 1/2 is arbitrary) and the LIA scaling k^2

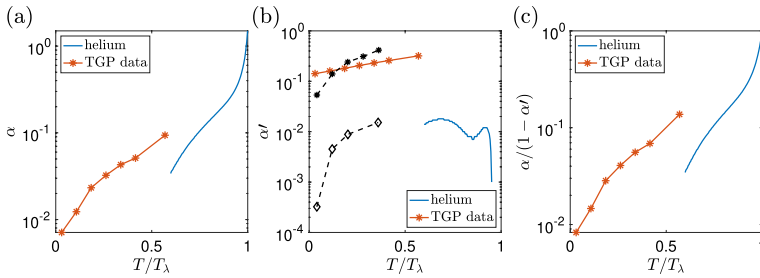


Fig. 9 Measured mutual friction coefficients obtained with the TGP model. We also plot the measured helium mutual friction coefficient taken from [45]. In figure (b), we also show the measured TGP friction coefficients for the case of the vortex lattice and a vortex ring presented in Fig. 9 (same markers)

In Fig. 8, we present the results of the fit. Figure 8a displays the coefficient λ_k for different temperatures. For comparison, we also plot the k^2 -scaling expected from the LIA model and Kelvin wave dispersion relation for GP KWs given by Eq. (11). A strong temperature dependence is observed, the higher the temperature, the larger the damping. Moreover, the scaling of λ_k seems in agreement with the SLIA prediction (33). Similarly, Fig. 8b displays the measured frequencies Ω_k . There is a small temperature dependence producing a slowdown of the frequency. In addition, it is clear that frequencies do not follow the LIA scaling, but they agree without adjustable parameters with the KW dispersion relation for the GP model. In Fig. 8c, d we show λ_k and Ω_k normalised by ω_k^{GP} . We then define the measured GP mutual friction coefficients by averaging over wave vectors $k/k_0 \in (2, 5)$ where curves are relatively flat. In addition, we average the ratio λ_k/Ω_k , that from Eq. (33) should be independent of the KW dispersion relation and equal to $\alpha/(1 - \alpha')$. Finally, the measured mutual friction coefficients are displayed in Fig. 9.

For comparison, we also plot the measured helium mutual friction coefficient taken from reference [45]. Helium and TGP mutual friction coefficient have been obtained at different temperature ranges. In the case of the TGP model, to perform the analysis carried out in this work at higher temperature is challenging, as thermal fluctuations become strong (including thermally excited vortices), which difficult the tracking of vortices.

The TGP-measured mutual coefficient α is remarkably of the same order of the one of helium, and it looks as a natural low-temperature continuation of the known (higher temperature) helium properties. On the contrary, the mutual friction coefficient α' seems not to agree with helium. Figure 9b also displays data from Fig. 5 (in black).

5 Discussion and Conclusions

First, we briefly reviewed some of the mutual friction effects on vortex lines and rings that are obtained in references [20] and [22]. In particular we reviewed the anomalous slowdown of rings that is produced by thermally excited Kelvin waves.

Then, we studied the effect of mutual friction and thermal noise on the relaxation of Kelvin waves on straight vortex lines by comparing the results of full 3D direct simulations of the TGP with a simple new LIA stochastic model with mutual friction and thermal noise included.

The new model allowed us to determine the mutual friction coefficient. By fitting the simple Langevin model prediction (35) to the TGP Kelvin wave correlation function shown in Fig. 8, we have successfully reproduced the TGP correlation functions.

The coefficients λ_k and Ω_k obtained from the fit show a distinct temperature dependence, and the values of the measured mutual friction coefficient α are of a similar order of magnitude as those measured in superfluid helium. However, the value of the mutual friction coefficient α' obtained from the fit deviates from the standard measurements. It is rather puzzling and important to note that the values of α' obtained in the TGP context for the vortex ring (reviewed above in section 3) also differed significantly, suggesting that the geometry of the vortex configuration can affect the mutual friction coefficients. However, as there is no direct link between the two methods of determining α' , this may just be a coincidence.

Finally, let us recall that to correctly describe superfluid liquid Helium, with a good equation of state and a dispersion relation with rotons, the GPE needs to be extended by including non-local and higher order nonlinear terms [46–48]. It is an open problem that is left for further study to see if such a more quantitative description still lead to the same results: a 'good' α and a 'bad' α' .

Acknowledgements G.K. was supported by the Agence Nationale de la Recherche through the project GIANTE ANR-18-CE30-0020-01. M.E.B. acknowledges support from the French Agence Nationale de la Recherche (ANR QUTE-HPC Project No. ANR-18-CE46-0013). This work was granted access to the HPC resources of GENCI under the allocation 2019-A0072A11003 made by GENCI. Computations were also carried out at the Mésocentre SIGAMM hosted at the Observatoire de la Côte d'Azur.

References

1. W.F. Vinen, J.J. Niemela, Quantum turbulence. *J. Low Temp. Phys.* **128**(5), 167–231 (2002). <https://doi.org/10.1023/A:1019695418590>
2. W.F. Vinen, D. Shoenberg, The detection of single quanta of circulation in liquid helium ii. *Proc. R. Soc. London Series A Math. Phys. Sci.* **260**(1301), 218–236 (1961). <https://doi.org/10.1098/rspa.1961.0029>
3. H.E. Hall, W.F. Vinen, D. Shoenberg, The rotation of liquid helium ii i. experiments on the propagation of second sound in uniformly rotating helium ii. *Proc. R. Soc. London Series A Math. Phys. Sci.* **238**(1213), 204–214 (1956). <https://doi.org/10.1098/rspa.1956.0214>
4. H.E. Hall, W.F. Vinen, D. Shoenberg, The rotation of liquid helium ii ii. the theory of mutual friction in uniformly rotating helium ii. *Proc. R. Soc. London Series A Math. Phys. Sci.* **238**(1213), 215–234 (1956). <https://doi.org/10.1098/rspa.1956.0215>
5. I. Bekarevich, I. Khalatnikov, Phenomenological derivation of the equations of vortex motion in He II. *Sov. Phys. JETP* **13**, 643–646 (1961)
6. K.W. Schwarz, Three-dimensional vortex dynamics in superfluid ^4He : line-line and line-boundary interactions. *Phys. Rev. B* **31**, 5782–5804 (1985). <https://doi.org/10.1103/PhysRevB.31.5782>
7. K.W. Schwarz, Three-dimensional vortex dynamics in superfluid ^4He : homogeneous superfluid turbulence. *Phys. Rev. B* **38**, 2398–2417 (1988). <https://doi.org/10.1103/PhysRevB.38.2398>

8. D. Kivotides, C.F. Barengi, D.C. Samuels, Triple vortex ring structure in superfluid helium II. *Science* **290**(5492), 777–779 (2000)
9. S. Yui, M. Tsubota, H. Kobayashi, Three-dimensional coupled dynamics of the two-fluid model in superfluid He 4: deformed velocity profile of normal fluid in thermal counterflow. *Phys. Rev. Lett.* **120**(15), 155301 (2018). <https://doi.org/10.1103/PhysRevLett.120.155301>
10. L. Galantucci, G. Krstulovic, C.F. Barengi, Friction-enhanced lifetime of bundled quantum vortices. *Phys. Rev. Fluids* **8**(1), 014702 (2023). <https://doi.org/10.1103/PhysRevFluids.8.014702>
11. L. Galantucci, A.W. Baggaley, C.F. Barengi, G. Krstulovic, A new self-consistent approach of quantum turbulence in superfluid helium. *Eur. Phys. J. Plus* (2020). <https://doi.org/10.1140/epjp/s13360-020-00543-0>
12. C.W. Gardiner, P. Zoller, Quantum kinetic theory. V. Quantum kinetic master equation for mutual interaction of condensate and noncondensate. *Phys. Rev. A* **61**, 033601 (2000)
13. C.W. Gardiner, J.R. Anglin, T.I.A. Fudge, The stochastic Gross-Pitaevskii equation. *J. Phys. B: At. Mol. Opt. Phys.* **35**, 1555–1582 (2002)
14. E. Calzetta, B.L. Hu, E. Verdaguer, Stochastic Gross-Pitaevsky equation for BEC via coarse-grained effective action. *Int. J. Mod. Phys. B* **21**, 4239–4247 (2007)
15. N.G. Berloff, M. Brachet, N.P. Proukakis, Modeling quantum fluid dynamics at nonzero temperatures. *Proc. Natl Acad. Sci.* **111**(1), 4675–4682 (2014). <https://doi.org/10.1073/pnas.1312549111>
16. C. Coste, Nonlinear Schrödinger equation and superfluid hydrodynamics. *Eur. Phys. J. B-Condens. Matter Compl. Syst.* **1**, 245–253 (1998)
17. M. Brachet, G. Sadaka, Z. Zhang, V. Kalt, I. Danaila. Coupling Navier-Stokes and Gross-Pitaevskii equations for the numerical simulation of two-fluid quantum flows. arXiv preprint [arXiv:2211.07361](https://arxiv.org/abs/2211.07361) (2022)
18. N.P. Proukakis, B. Jackson, Finite-temperature models of Bose-Einstein condensation. *J. Phys. B* **41**(20), 203002 (2008). <https://doi.org/10.1088/0953-4075/41/20/203002>
19. M.J. Davis, S.A. Morgan, K. Burnett, Simulations of bose fields at finite temperature. *Phys. Rev. Lett.* **87**(16), 160402 (2001). <https://doi.org/10.1103/PhysRevLett.87.160402>
20. G. Krstulovic, M. Brachet, Energy cascade with small-scale thermalization, counterflow metastability, and anomalous velocity of vortex rings in Fourier-truncated Gross-Pitaevskii equation. *Phys. Rev. E* **83**(6), 066311 (2011). <https://doi.org/10.1103/PhysRevE.83.066311>
21. G. Krstulovic, M. Brachet, Dispersive bottleneck delaying thermalization of turbulent Bose-Einstein condensates. *Phys. Rev. Lett.* **106**, 115303 (2011). <https://doi.org/10.1103/PhysRevLett.106.115303>
22. G. Krstulovic, M. Brachet, Anomalous vortex-ring velocities induced by thermally excited Kelvin waves and counterflow effects in superfluids. *Phys. Rev. B* **83**, 132506 (2011). <https://doi.org/10.1103/PhysRevB.83.132506>
23. E.P. Gross, Structure of a quantized vortex in boson systems. *Il Nuovo Cimento* (1955-1965) **20**(3), 454–477 (1961). <https://doi.org/10.1007/BF02731494>
24. L. Pitaevskii, Vortex lines in an imperfect Bose gas. *Sov. Phys. JETP* **13**(2), 451–454 (1961)
25. C. Nore, M. Abid, M.E. Brachet, Decaying kolmogorov turbulence in a model of superflow. *Phys. Fluids* **9**(9), 2644–2669 (1997). <https://doi.org/10.1063/1.869473>
26. C. Nore, M. Abid, M. Brachet, Kolmogorov turbulence in low-temperature superflows. *Phys. Rev. Lett.* **78**(20), 3896–3899 (1997). <https://doi.org/10.1103/PhysRevLett.78.3896>
27. C. Nore, M. Brachet, S. Fauve, Numerical study of hydrodynamics using the nonlinear Schrödinger equation. *Phys. D* **65**(1–2), 154–162 (1993)
28. P. Gérard, The cauchy problem for the Gross-Pitaevskii equation. *Annales de l'Institut Henri Poincaré C, Analyse non linéaire* **23**(5), 765–779 (2006). <https://doi.org/10.1016/j.anihpc.2005.09.004>
29. R.J. Donnelly, *Quantized Vortices in Helium II* (Cambridge University Press, 1991)
30. W. Thomson, Vibrations of a columnar vortex. *London Edinburgh Dublin Philos. Mag. J. Sci.* **10**(61), 155–168 (1880). <https://doi.org/10.1080/14786448008626912>
31. P.H. Roberts, On vortex waves in compressible fluids II. The condensate vortex. *Proc. R. Soc. London Series A Math. Phys. Eng. Sci.* **459**(2031), 597–607 (2003). <https://doi.org/10.1098/rspa.2002.1033>
32. U. Giuriato, G. Krstulovic, S. Nazarenko, How trapped particles interact with and sample superfluid vortex excitations. *Phys. Rev. Res.* **2**, 023149 (2020). <https://doi.org/10.1103/PhysRevResearch.2.023149>
33. L.S. Da Rios, Sul moto d'un liquido indefinito con un filetto vorticoso di forma qualunque **22**(1), 117–135. <https://doi.org/10.1007/BF03018608>

34. D. Gottlieb, S.A. Orszag, *Numerical Analysis of Spectral Methods* (SIAM, Philadelphia, 1977)
35. G. Krstulovic, A theoretical description of vortex dynamics in superfluids. kelvin waves, reconnections and particle-vortex, Habilitation à diriger des recherches. Université Côte d'Azur. (2020)
36. C. Connaughton, C. Josserand, A. Picozzi, Y. Pomeau, S. Rica, Condensation of classical nonlinear waves. *Phys. Rev. Lett.* **95**(26), 263901 (2005). <https://doi.org/10.1103/PhysRevLett.95.263901>
37. N.G. Berloff, A.J. Youd, Dissipative dynamics of superfluid vortices at nonzero temperatures. *Phys. Rev. Lett.* **99**(14), 4 (2007). <https://doi.org/10.1103/PhysRevLett.99.145301>
38. C. Nore, M.E. Brachet, E. Cerda, E. Tirapegui, Scattering of first sound by superfluid vortices. *Phys. Rev. Lett.* **72**, 2593–2595 (1994). <https://doi.org/10.1103/PhysRevLett.72.2593>
39. L. Kiknadze, Y. Mamaladze, The waves on the vortex ring in He ii. *J. Low Temp. Phys.* **126**(1–2), 321–326 (2002)
40. C.F. Barenghi, R. Hanninen, M. Tsubota, Anomalous translational velocity of vortex ring with finite-amplitude kelvin waves. *Phys. Rev. E* **74**(4), 046303 (2006). <https://doi.org/10.1103/PhysRevE.74.046303>
41. U. Giuriato, G. Krstulovic, Interaction between active particles and quantum vortices leading to Kelvin wave generation. *Sci. Rep.* **9**(1), 4839 (2019). <https://doi.org/10.1038/s41598-019-39877-w>
42. G. Krstulovic, Kelvin-wave cascade and dissipation in low-temperature superfluid vortices. *Phys. Rev. E* **86**(5), 055301 (2012). <https://doi.org/10.1103/PhysRevE.86.055301>
43. A. Villois, G. Krstulovic, D. Proment, H. Salman, A vortex filament tracking method for the Gross–Pitaevskii model of a superfluid. *J. Phys. A: Math. Theor.* **49**(41), 415502 (2016). <https://doi.org/10.1088/1751-8113/49/41/415502>. (Accessed 2020-02-29)
44. U. Giuriato, G. Krstulovic, Stochastic motion of finite-size immiscible impurities in a dilute quantum fluid at finite temperature. *Phys. Rev. B* **103**, 024509 (2021). <https://doi.org/10.1103/PhysRevB.103.024509>
45. R.J. Donnelly, C.F. Barenghi. The observed properties of liquid helium at the saturated vapor pressure. *J. Phys. Chem. Reference Data* **27**(6), 1217–1274 (1998). <https://doi.org/10.1063/1.556028>. tex.eprint: https://pubs.aip.org/aip/jpr/article-pdf/27/6/1217/11342901/1217_1_online.pdf
46. N.G. Berloff, P.H. Roberts, Motions in a bose condensate: VI. Vortices in a nonlocal model. *J. Phys. A Math. General* **32**(30), 5611–5625 (1999). <https://doi.org/10.1088/0305-4470/32/30/308>
47. N.P. Müller, G. Krstulovic, Critical velocity for vortex nucleation and roton emission in a generalized model for superfluids. *Phys. Rev. B* **105**(1), 014515 (2022). <https://doi.org/10.1103/PhysRevB.105.014515>
48. N.P. Müller, G. Krstulovic, Kolmogorov and Kelvin wave cascades in a generalized model for quantum turbulence. *Phys. Rev. B* **102**(13), 134513 (2020). <https://doi.org/10.1103/PhysRevB.102.134513>

Publisher's Note Springer Nature remains neutral with regard to jurisdictional claims in published maps and institutional affiliations.

Springer Nature or its licensor (e.g. a society or other partner) holds exclusive rights to this article under a publishing agreement with the author(s) or other rightsholder(s); author self-archiving of the accepted manuscript version of this article is solely governed by the terms of such publishing agreement and applicable law.